Journal of Civil Engineering, Science and Technology
Volume 10, Issue 1, April 2019

PREDICTING THE STRUCTURAL PERFORMANCE OF SANDWICH CONCRETE PANELS SUBJECTED TO BLAST LOAD CONSIDERING DYNAMIC INCREASE FACTOR

M. Hanifehzadeh[1*] and M. M. R. Mousavi[2]
[1]Sonny Astani Department of Civil and Environmental Engineering, University of Southern California, Los Angeles, CA, USA
[2] Department of Civil and Environmental Engineering, University of Houston, Houston, TX, USA

Date received: 06/11/2018, Date accepted: 22/02/2019
*Corresponding author's email: hanifehz@usc.edu
https://doi.org/10.33736/jcest.1067.2019

Abstract - The safety of civil structures can be significantly improved against shock waves and blast loads by using steel concrete steel (SCS) protective walls. A numerical study was performed to simulate the response of SCS wall subjected to a near-field blast load. A conventional SCS panel subjected to near-field blast load and its structural performance had been evaluated in terms of maximum damage and deformation. The simulations were performed using ABAQUS\EXPLICIT finite element package and built-in concrete damage plasticity concrete constitutive formulation. The dynamic increase factor (DIF) was added to the material constitutive behaviour to consider the rate effect on the behaviour of concrete and steel. The maximum deformation, the plastic strain, and the failure mode under different loading scenarios were investigated. This study predicts the structural response of the SCS panel with different blast charge and identification of optimum configuration in terms of concrete strength and plate thickness. In the second part of the study, two novel sandwich configurations consisting of a corrugated metal sheet and the concrete core are proposed and compared with the conventional protective walls. The optimum parameters for each structural component are identified using an optimization procedure. Based on this study, the proposed wall configuration shows more damage tolerance subjected to the blast loading as well as less out of plane deformation and weight compared to the conventional walls.

Keywords: Sandwich panel, blast load, finite element analysis, concrete damage plasticity

1.0 INTRODUCTION

Explosions due to terrorist attacks can induce catastrophic damages to the buildings, bridges, and infrastructure. To minimize the consequences of the air blast loads on buildings, application of steel-concrete steel (SCS) composite panel, significantly improves the structural safety. In using SCS panels, the ductility of member significantly increases, and progressive collapse and sudden failure could be prevented. Blast load with sudden release of energy is due to chemical or nuclear source that causes large deformation. The blast induces shock wave traveling in the radial direction from the source detonation. For maximum performance in case of blast load, both the strength and ductility of a member should be improved. SCS panel consists of two steel plates with a concrete core in between. The composite performance between the plates and the concrete layer is achieved by steel connectors welded to the plate's inner surface. The connectors provide full contact and shear transfer between the plates and the core. The SCS panels have considerable advantages over the reinforced (RC) panels in terms of cost and time of construction as it could be prefabricated. In addition, the two steel plates act as formwork which promotes the construction efficiency in onsite fabrication. The plates also provide confinement for the core and improve the compressive strength of concrete. Therefore, SCS panels have more structural stiffness and ductility. In terms of dynamic performance, the high density of the concrete provides inertia force improving blast resistance compared to a single steel plate. The panels could be used in military shelters and nuclear power plants station or barriers for protection of the building and critical infrastructures [1-3]. Wang et al. [4] studied the performance of curved SCS panel used for offshore structures and identified different failure modes. They identified the shear connector as a vital parameter in the composite performance of the panel. They evaluated the effect of rising height (or rise to span ratio) and rear to front plate thickness ratio. They concluded that increase in rise height and front plate thickness can improve the overall response of the panel. Castedo et al. [5] performed an experimental and numerical

study on slabs reinforced with steel and polypropylene and used non-destructive tests to characterize the damage. Athanasiou et al. [6] used LS-DYAN to study the effect of near-field blast on a two-layered reinforced RC slab with different detonation charge. They validated their results with experimental data and observed that the failure mode shifts from penetration to perforation by increasing the blast charge amount. Kong et al. [7] performed a numerical investigation non-composite SCS panel without a shear connector. They proposed a novel detailing for flared end connections to eliminate relative movement between the concrete core and the steel plates through axial restraint. They found that the shear connection between the core and the plate is insignificant under dynamic load. Tabatabaei et al. [8] performed experimental and numerical study concrete panel reinforced with two types of carbon fibres. They fabricated a 1830x1830 mm steel reinforced panel for the experiment under the net equivalent weight of 34 kg of TNT charge and at standoff distances of 1065 mm and 1370 mm. They found that the addition of carbon fibre significantly reduced the cracking and spalling of the concrete up to 89%. A numerical study performed using LS-DYNA and material model 159 for concrete to develop spall prediction curve based on the thickness of the slab to standoff distance ratio. Hanifehzadeh et al. [9] studied the dynamic structural performance of the sandwich panel under high strain rate load using concrete damage plasticity and Smoothed Particle Hydrodynamics (SPH) technique. The results showed that the CDP model offers faster analysis with reliable results compared to SPH. Sawab et al. [10] and [11] performed an experimental and numerical study on the sandwich panels fabricated using ultra-high performance concrete (UHPC) used for the small modular reactor. They obtained the optimum reinforcement configurations for maximum shear performance.

This study evaluated the blast resistivity of SCS panel using non-linear explicit finite element analysis and elaborates the advantages of the SCS panels compared to regular RC panels and walls. A novel composite configuration consists of concrete core and the corrugated metal sheet is proposed for blast protection application. Two-panel configurations with the same boundary conditions and similar geometry were developed including conventional SCS wall and two novel composite walls. The structural responses of the walls were optimized and compared with conventional versions. The proposed configurations showed considerable improvement in terms of structural performance, when compared to conventional designs.

2.0 FINITE ELEMENT ANALYSIS

Numerical analysis of the blast loading was performed using explicit solver of the ABAQUS FEA package[12]. The geometry of the model consisted of a solid 3000x3000 mm concrete core with 300 mm thickness sandwiched between two steel plates. 3D continuum brick elements with linear shape function and reduced integration (C3D8R) were used to mesh the core. 201,600 elements were used for the plates considering the small thickness. The location of blast detonation is at the center of the wall with a standoff distance of 10 m. Fixed boundary condition was considered on the edges where the displacement of the nodes was restrained. It is assumed that the core is fully connected to the plates using shear studs or j-hooks during the construction process. Therefore, the plates were modeled using 4-noded shell elements (S4R) tied to the surface of the concrete core. The general configuration of the model is illustrated in Figure 1.

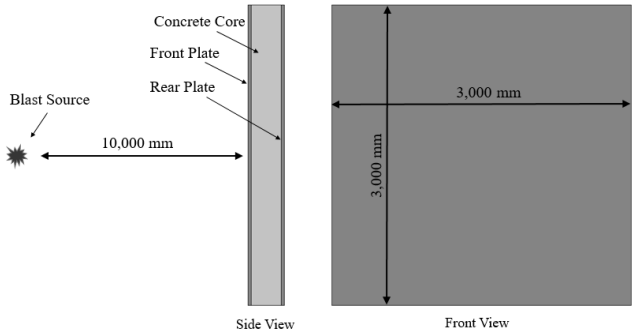

Figure 1 The geometry of the RC panel and blast detonation source.

3.1 MATERIAL MODEL

3.1.1 CONCRETE

Concrete Damage Plasticity (CDP) proposed by Lee and Fenves [13] built-in ABAQUS [14] was assigned to the concrete wall. The uniaxial compressive strength of concrete was taken as 50 MPa. The CDP constitutive behavior has been successfully utilized in many blast, impact and nonlinear analysis cases [15-19]. The compressive and tensile behavior in uniaxial direction is shown in Figure 2. In tension, the stress-strain response is linear until σ_{co} where the micro cracks initiate in the concrete volume. Here, σ_{co}, linear proportional limit, was taken as 60% of the maximum compressive strength. σ_{cu} is the maximum uniaxial strength derived from the uniaxial compression experiment on concrete the cylinder. Beyond that, micro cracks join and interact and will lead to dilative behaviour in concrete. The stress-strain showed softening behaviour under this condition and the material was considered as failed. In the tension, strain hardening did not exist in the model and the softening was observed immediately after the linear proportional limit.

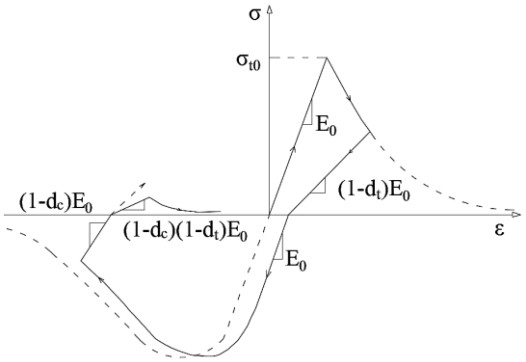

Figure 2 Behaviour of concrete under uniaxial compression and tension [14].

The model also implemented scaler damage in both tension and compression assigned from zero to one by two damage variables, d_t, and d_c. Zero represents the undamaged material and one represents total loss of strength. The stress-strain relations under uniaxial tension and compression are formulated as

$$\sigma_c = (1 - d)E_0(\varepsilon_c - \varepsilon_c^p) \quad (1)$$

$$\sigma_t = (1 - d)E_0(\varepsilon_t - \varepsilon_t^p) \quad (2)$$

where E_0, ε_c^p and ε_t^p are the initial elastic stiffness of the concrete, the equivalent plastic strain in compression and tension, respectively. The default parameters of the model calibrated for grade 50 concrete is summarized in Table 1 [20]. Young's modulus is determined using the equation of $E = 4700\sqrt{f_c'}$ proposed by ACI-318 [21] where f_c' is uniaxial compressive strength of concrete cylinder in MPa. The strain the maximum strength, ε_0', and ultimate strain, ε_{cu}, are assumed as 0.002 and 0.0035 respectively. The maximum tensile strength is assumed as 10% of compressive strength.

Table 1 Input parameters for the CDP model.

Parameter	Value
Dilation angle	16
Eccentricity	0.1
f_{b0}/f_{c0}	1.16
K	0.667
Viscosity parameter	0.0001
Compressive strength (MPa)	50
Tensile Strength (MPa)	5
Young's Modulus (GPa)	27.8
Poisson's Ratio	0.21

3.1.2 STEEL

Elasto-plastic behavior with isotropic hardening was assumed for the steel sections. The A36 material was considered for the steel with Young's modulus and Poisson's ratio considered as 200 GPa and 0.3. The input parameters for the steel model are summarized in Table 2.

Table 2 Material properties for steel

Part	Density [kg/m^3]	Yield stress [MPa]	Ultimate strength [MPa]	Elastic modulus [GPa]	Poisson's ratio	Maximum plastic strain
Steel plate	7800	250	360	200	0.3	0.20

3.1.3 DYNAMIC INCREASE FACTOR

Increase in strength for steel and concrete under high strain rate has been reported by many researchers which are mostly contributed to inertia effect [22-24]. The dynamic increase factor (DIF) is generally used in blast and impact problems defined as strength under dynamic load with respect to static strength. In the blast case, the rate may reach up to 10^3 sec^{-1} as shown in Table 3.

Table 3 Strain rate for different phenomena [25].

Loading Scenario	Strain Rate [sec^{-1}]
Creep	$-\infty$ - 10^{-8}
Quasi-static	10^{-6} - 10^{-4}
Earthquake	10^{-3} - 10^{-2}
Impact	10^{1} - 10^{2}
Blast	10^{2} - 10^{3}

In this study, the CEB-FIP recommended model [26] used for concrete strength for compression and tension as

$$DIF_{comp.} = \gamma \left(\frac{\dot{\varepsilon}_d}{\dot{\varepsilon}_s}\right)^{1/3} \quad for\ \dot{\varepsilon} > 30s^{-1} \tag{3}$$

$$\log\gamma = 6.156\alpha - 2 \tag{4}$$

$$\alpha = 1/(5 + \frac{9f_c'}{f'_0}) \tag{5}$$

$$DIF_{ten.} = \beta \left(\frac{\dot{\varepsilon}_d}{\dot{\varepsilon}_s}\right)^{1/3} \quad for\ \dot{\varepsilon} > 30s^{-1} \tag{6}$$

$$\log\beta = 7.11\delta - 2.33 \tag{7}$$

$$\delta = 1/(10 + \frac{6f_c'}{f'_0}) \tag{8}$$

where $\dot{\varepsilon}_d$, $\dot{\varepsilon}_s$ and f'_c are the dynamic strain rate, the quasi-static strain rate (taken as 30×10^{-6} s^{-1}) and quasi-static unconfined compressive strength. f'_0 is a constant value equal to 10 MPa. For the steel, the equation proposed by Cowper and Symonds [27] used to calculate DIF as

$$DIF = 1.0 + \left(\frac{\dot{\varepsilon}}{C}\right)^{\frac{1}{q}} \tag{9}$$

where $\dot{\varepsilon}$ is strain rate, and C and q are constants values taken as 40.4 and 5 for mild steel. Considering conservative strain rate of 100 s^{-1} and using Eqn. 3 and Eqn. 6, the DIF for concrete was obtained as 2.11 and 2.44 in compression and tension. Similarly, DIF was calculated as 1.65 for the steel plates form Eqn.

9. The quasi-static strength of material reported in section 2.3 and 2.4 were multiplied by the pertinent DIF before implementing in the finite element model.

4.0 BLAST LOAD

A large amount of energy released abruptly from explosion induces a pressure wave, which propagates through the surrounding environment in a blast incident. The pressure behind the shock wave drops below the atmospheric pressure called negative pressure phase. Consequently, a vacuum zone forms on the structure surface, applying a force in the reversed direction of the shock wave. Maximum applied force on the structure is a function of explosive mass defined as kg of TNT and distance from the source. A general pressure time history of a shock wave is shown in Figure 3.

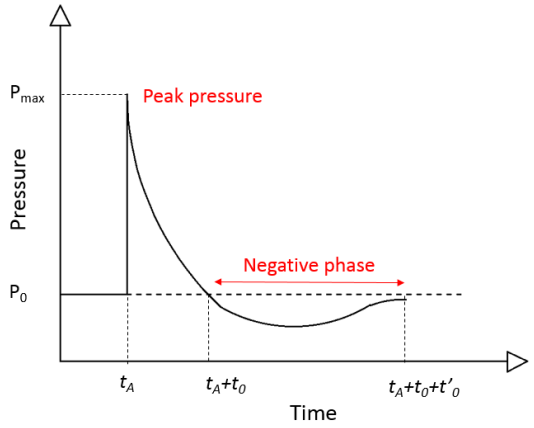

Figure 3 Shock wave time history [14].

P_0 is the atmospheric pressure and P_{max} is overpressure peak caused by the shock arrived at time t_A. The duration of the vacuum phase is shown with t'_0 in Figure 3. Built-in blast function CONWEP developed by Kingery and Bulmash [28] was used to apply the shock wave to the panel. The amount of blast charge, the location of the detonation, and the subjected surface should be identified by the user. For this study, 10 kg TNT with standoff distance of 10 m was considered as the base case loading scenario. The panels were subjected to different blast charges and the responses are compared in section 5.1. In this study, only the effect of pressure from the blast incident was applied to the panels. The modeling techniques for the combined effect of mechanical force and high temperature could be found in Zeng et al. [29] and Talebi et al. [30, 31].

5.0 RESULTS

The results of the analysis for the conventional geometry are provided in this section. The plastic equivalent strain (PEEQ) and iso-surface compressive damage subject to 10kg detonation charge are shown in Figure 4 and Figure 5. The damage is initiated at the corner and edges considering fixed BC and then propagates through the center of the panel. The rear panel is yielded during the impact due to the large deformation, therefore only the PEEQ is shown in this section.

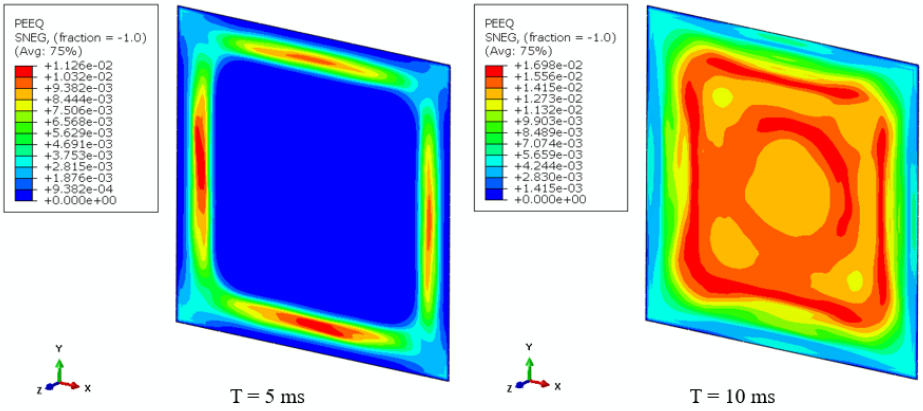

Figure 4 Equivalent plastic strain on the rear plate

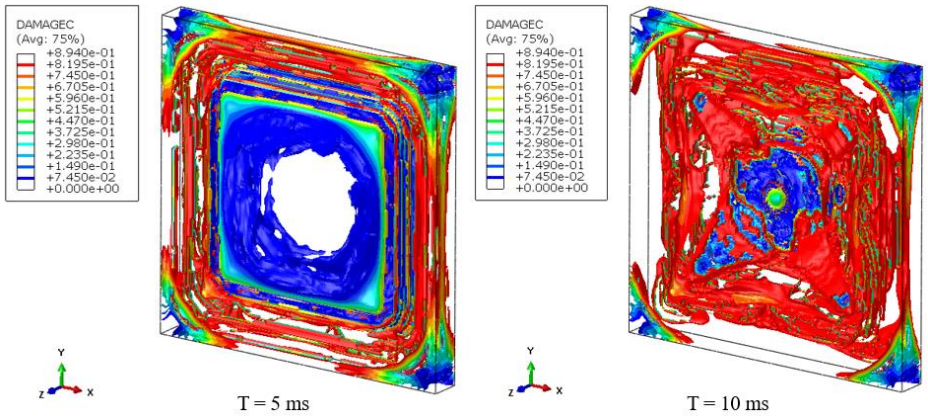

Figure 5 Iso-surface compressive damage in the concrete core.

5.1 BLAST CHARGE

In this section, the panel is subjected to four blast loads with a different charge ranging from 2 to 20 kg of TNT. The responses of the panels are compared in Figure 6. The maximum out of plane deformation and PEEQ are provided in Table 4. The results show that the rear plate is not yielded under 2 kg blast.

Table 4 Structural response of steel plate under different shock wave.

Blast Charge [kg]	Deformation [mm]	PEEQ
2	29	0.0
5	97	0.0001
10	175	0.0290
20	335	0.0625

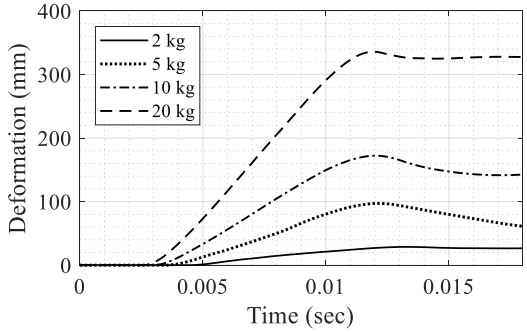

Figure 6 Deformation time history at the center of the rear panel.

5.2 COMPOSITE BEHAVIOR

In this section, the effect of composite behavior of the panel on the maximum deformation is investigated. This is important considering the extra cost of j-hooks installation required for composite interaction. For full composite behavior, adequate number of j-hooks is required to be welded on both rear and front plates which can significantly increase the total cost of fabrication of the panel. For this purpose, the analysis is performed for two cases; with and without a full bond between the core and plates. Tie command is used in the fully connected condition to tie the nodes in the core and plates. In the second scenario, only surface to surface friction with a coefficient of 0.2 is considered between the core and the plates. The results show 16% improvement in rear deformation in the fully connected scenario, as shown in Table 7.

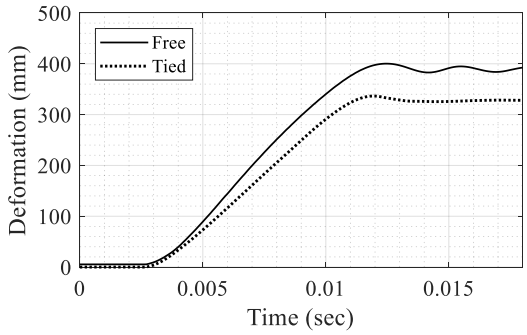

Figure 7 The effect of composite behavior on the rear deformation of the panel (20 kg charge).

5.3 CONCRETE DENSITY

Several researchers have reported higher resistance against dynamic load considering the inertia force of the concrete core. Here, the effect of density evaluated in the response of sandwich panel was subjected to 20 kg charge. Four different cases covering light, normal, and heavy weight concretes were considered and the results are summarized in Table 5 and Figure 8.

Table 5 The effect of concrete density on the structural response.

Case	Concrete density [kg/m^3]	Max. Rear deformation [mm]
1	1,300	384
2	1,800	357
2	2,300	335
3	2,800	316
4	3,300	302

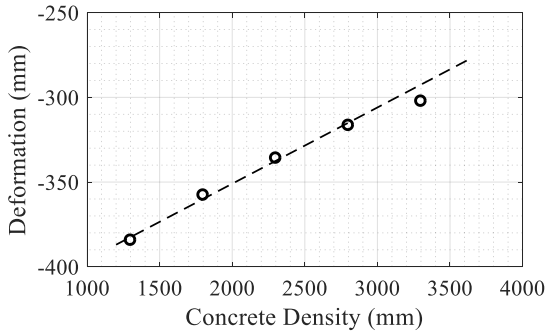

Figure 8 Rear deformation versus concrete density.

In Figure 8, linear behavior between density and rear deformation was observed. By using heavy concrete

instead of normal weight and increasing the density by 43%, the rear deformation is reduced only by 10%. It is concluded that the effect of density is insignificant and therefore; density is not considered in the optimization process in section 6.

5.4 STEEL PLATE THICKNESS

A test matrix is developed to optimize the configuration of the wall in terms of plate thickness which is shown in Table 6. For better comparison, the sum of the thickness of the front and rear plates was fixed for all cases. The maximum out of plane deformation at the center of the wall considered as the controlling parameter for the optimization process. The failure at the rear plate is considered as the failure of the wall. In the sandwich configuration, the concrete core may experience severe damage; however, while the rear plate is not ruptured, the structure could be assumed in a safe condition. The deformation time history for five cases in Table 6 is shown in Figure 9.

Table 6 optimization matrix for sandwich configuration (10 kg charge).

Case	Front Thickens [mm]	Rear Thickness [mm]	Rear to Front Thick. Ratio	Maximum Rear Deformation [mm]
1	50	12	0.24	213
2	38	24	0.63	184
3	32	32	1.00	175
4	24	38	1.58	163
5	12	50	4.16	159

Based on the results, the rear deformation is highly a function of rear thickness. Larger rear thickness reduces the deformation with a quadratic rate (see Figure 10). However, the deformation tends to converge with a ratio of the rear to front thickness beyond 1.5. Therefore, this value could be considered as the optimum thickness ratio.

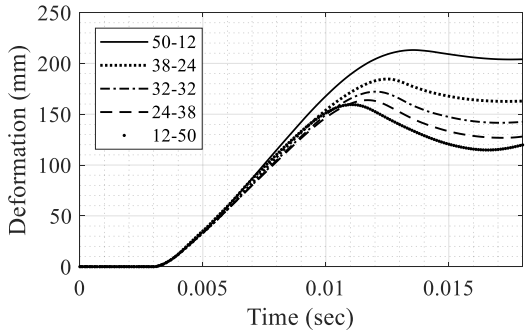

Figure 9 Rear deformation for different plate thickness configuration (10 kg charge).

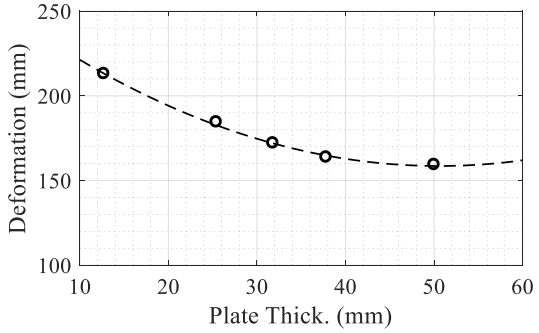

Figure 10 Rear deformation versus rear plate thickness (10 kg charge).

4.5 CONCRETE STRENGTH

The effect of concrete strength on the performance of the panel is studied in this section. For this purpose, a range of concrete strength from conventional up to high-strength is considered for the concrete core. The material properties and input parameters for normal strength and high-strength concrete calibrated to be used in the CDP model could be found in Shafiefar et al. [32], Sawab et al. [33], Hanif et al. [34] and Baghi et al.[35]. The effect of concrete strength is shown in Figure 11. The variation of rear deformation with respect to concrete strength is shown in Figure 12. It could be seen from the figure that increasing concrete increased the strength from 35 MPa to 100 MPa, which further reduced the rear deflection from 188 to 123 mm.

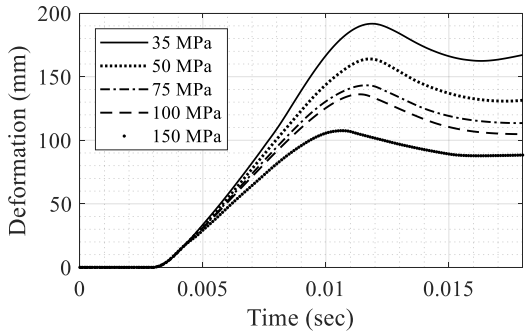

Figure 11 Rear deformation for different compressive strength (10 kg charge).

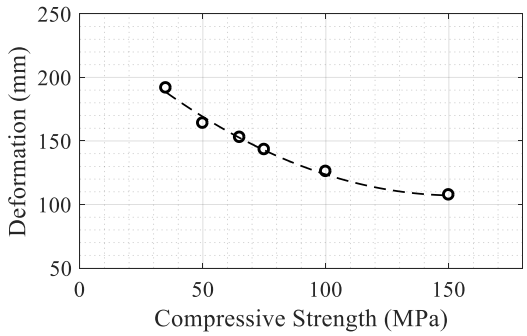

Figure 12 Rear deformation versus rear compressive strength (10 kg charge).

5.0 MESH SENSITIVITY

The mesh sensitivity studies on the model have been performed for 10 kg charge and 10 m standoff distance, wherein the optimal mesh size was selected accordingly. Mesh size needs to be optimized to avoid excessive cost of computation and also to avoid loss of accuracy. Mesh size of 25 mm for the concrete core is considered in order to provide 12 elements through the thickness. The rear and front plate have 25 mm mesh size as well.

Table 7 Results of mesh sensitivity study.

Case	Number of Elements	Concrete Element Size [mm]	No. of Elements Through the Depth	Rear Deformation [mm]	PEEQ
1	382,500	20	15	175	0.0120
2	201,600	25	12	175	0.0117
3	28,800	50	6	172	0.0111

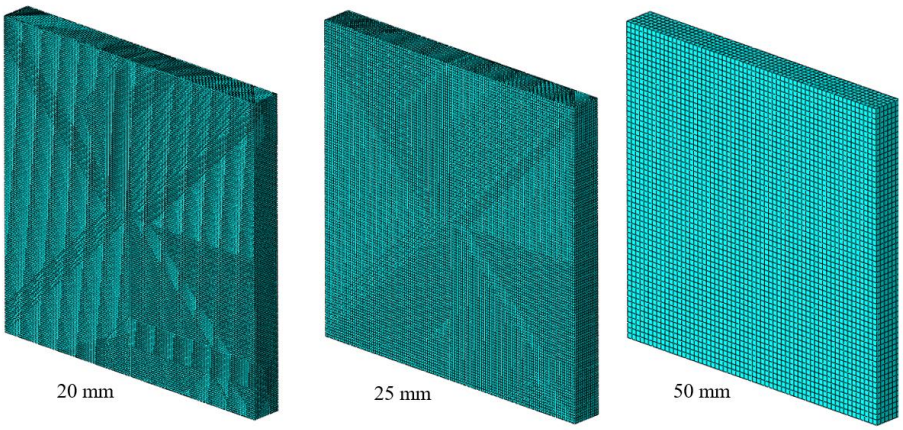

Figure 13 mesh density of the concrete core.

6.0 PROPOSED CONFIGURATION

Based on the results obtained from the previous sections, two novel composite sandwich panels have been introduced to improve the structural performance of the wall against blast load. The two governing factors for optimum configuration is the total weight of the panel and minimum out of plane deformation at the center. The front and rear steel plates are considered for the new panel to minimize the risk of scabbing and fragmentation. The core concrete provides inertia force required to minimize the out of plane deformation. Furthermore; the presence of steel plates improves the concrete strength by providing passive confinement.

6.1 SERIES CONFIGURATION

The first model consists of a concrete core and a corrugated metal sheet. Considering flexural behavior, the concrete core is placed in the compressive area and a thick plate is placed on the rear which is the tensile region. The corrugated steel plate transfers the shear force from the core to the rear plate to maintain composite interaction. In the ultimate level of deformation, the energy dissipation capability of the corrugated steel wall provides further resistance against the shock wave. Since the concrete core is enclosed between the two steel plates, no scabbing is predicted in the rear face of the current configuration. The geometry of the proposed wall is shown in Figure 14. Due to the modular configuration of the system, it can be pre-fabricated in the factory to reduce cost and save fabrication time. Since the concrete core performs well in the compressive region, the thickness of the front plate could be reduced for weight and cost optimization.

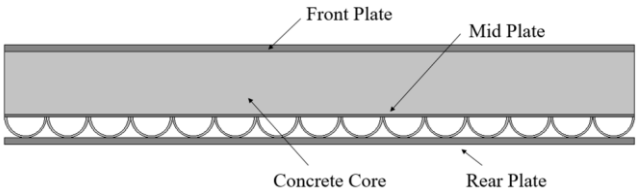

Figure 14 First proposed configuration for the shock resistance composite wall.

A series of analysis with different plate thicknesses of the front, damper and rear plate is performed to identify the optimum plate thickness for the composite wall, as shown in Table 8. In order to maintain total weight and weight of the steel in the wall, the sum of the steel plates thicknesses is limited to 60 mm in the parametric analysis. Since the rear plate has a major role in the general response of the wall maximum thickness of 30 mm is considered in the parametric study. Thicknesses higher than 30 mm is not considered since the cost of material will significantly increase. Since the mid plate is close to the neutral axis, the value of 10 mm is considered, which refers to the minimum value. Cases 3 and 5 in the table have the minimum rear deformation under the blast load. Although the composite wall has a higher cost of fabrication, the rear deformation is 29 % and 22% less than the conventional wall for 10 kg and

20 kg respectively. Based on the results in section 7.2, the same deformation could be obtained from the conventional wall if the concrete is increased from 50 MPa to 115 MPa, which results in an additional cost of fabrication. The out of plane deformations of the panel under 10 kg and 20 kg blast charge are shown in Figure 15. The parametric analysis performed on the steel plate thickness and deformation of the proposed model for case 3 under 10 kg and 20 kg blast charge are shown in Table 8 and Figure 15.

Table 8 Parametric analysis of plate thickness (20 kg charge).

Case	Front Plate Thick. [mm]	Damper Plate Thick. [mm]	Rear Plate Thick. [mm]	Rear Deformation [mm]
1	10	10	30	284
2	5	20	30	295
3	10	15	30	261
4	15	10	30	275
5	20	5	30	263

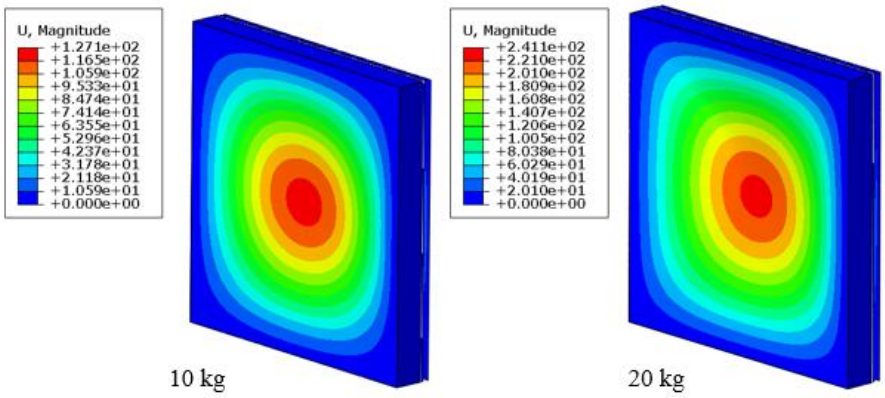

Figure 15 Out of plane deformation of the composite panel under 10 kg and 20 kg blast charge at t=1 ms for the case 3.

6.2 PARALLEL CONFIGURATION

The main idea behind the second configuration is to increase the flexural stiffness of the panel using the composite interaction between wide flange steel sections, steel plate, and concrete core. As shown in Figure 16, wide flange sections are considered between the two steel plates and the concrete is casted in the cavities. The steel sections and the plates provide confinement in three directions for the concrete core. On the other hand, the concrete core provides confinement for the steel sections and prevents local buckling of the web. Two options are available to provide composite interaction in the system; welding the flange to the plates or installation j-hooks or shear studs on the inner surface of the steel plates. In the first option, the shear is transferred by the web of the steel sections, while in the second option, the shear is transferred through the concrete segments in the presence of j-hooks.

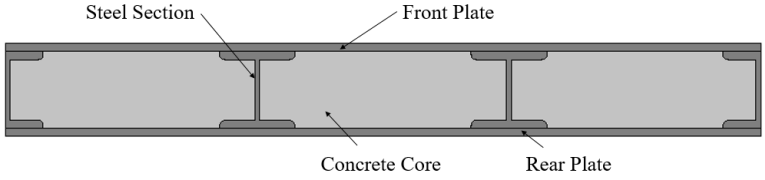

Figure 16 Second proposed configuration for the shock resistance composite wall.

The current configuration has the same geometry as in the conventional sandwich panels, while the rear deformation is significantly reduced up to 42% (case 3 under 10 kg charge). Comparison of the deformation between different cases could be conducted, as shown in Table 9, where three different steel

sections as well as two front steel thickness were analyzed. Maximum rear plate thickness of 30 mm is considered for all the cases. Figure 17 shows the deformation of the panel under 10 kg and 20 kg blast charge.

Table 9 Parametric analysis of steel section (10 kg).

Case	Section	Front Plate Thick. [mm]	Flange Thick. [mm]	Web Thick. [mm]	Rear Deform. [mm]
1	W12X14	30	5.7	5.1	157
2	W12X50	30	16.3	9.4	133
3	W12X136	30	31.8	20.1	101
4	W12X50	20	16.3	9.4	194
5	W12X136	20	31.8	20.1	116

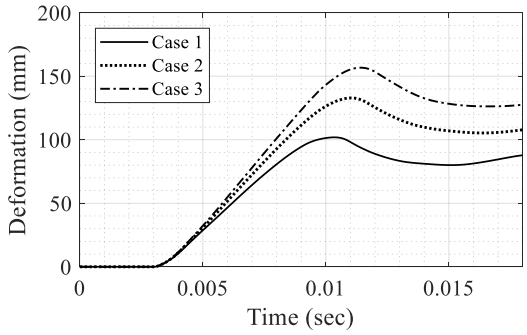

Figure 17 Rear deformation for steel sections (10 kg charge).

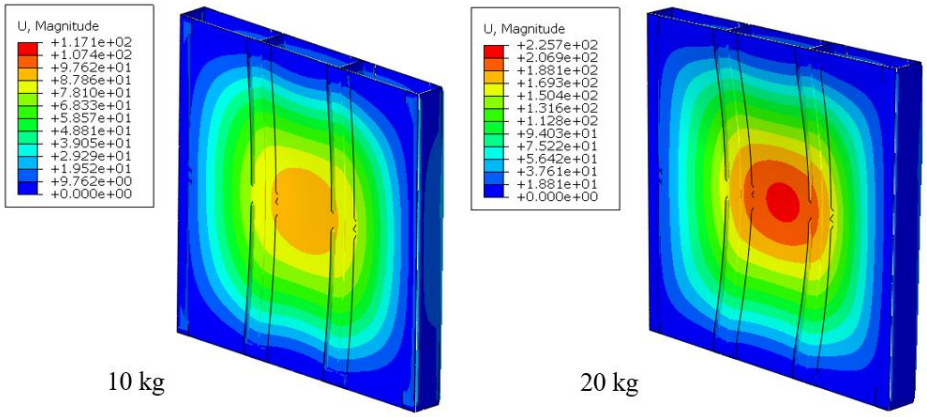

Figure 18 Out of plane deformation of the composite panel under 10 kg and 20 kg blast charge at t=1 ms for case 3.

7.0 SUMMARY OF THE RESULTS AND DISCUSSION

Summary of the results for different configurations is provided in Table 10 for better comparison. The second proposed model or parallel model has the best structural performance in terms of out of plane deformation. The weight of the steel parts and the total weight of the panels are in a similar range in Table 10, while the out of plane deformation for the second configuration is significantly less. This improvement could be attributed to the composite interaction between the steel and concrete. In the series model, the corrugated section experienced buckling at the center especially in the higher level of deformation. This issue increased the overall deformation of the wall. Considering brittle behavior of the concrete, in a high level of deformation, the resistance of the core reduced significantly. Therefore, the key to obtain the maximum capacity is obtaining the highest initial flexural stiffness, which is based on the results observed

in the second model. It was found that the initial resistance against the blast load is provided by the concrete core, while the rear steel plate provides final resistance in a higher level of deformation. The cost of material is expected to be almost equal between the conventional SCS wall and the parallel model. Note that in the conventional model, a considerable number of shear studs or J-hooks needs to be installed on both steel plates to provide composite interaction between the concrete and the plates. However, in the parallel model, there is no need for inclusion of shear studs since the shear is transferred through the steel section. Based on the results presented in Table 8, the average reduction of deformation is about 34% in the parallel configuration.

Table 10 Summary of the results.

Configuration	Reference	Case	Total weigh (kg)	Weight of steel (kg)	5 kg charge	10 kg charge	20 kg charge
Conventional SCS	Table 6	3	10,730	4,520	97	175	336
Series	Table 8	3	11,200	4,990	60	124	261
Parallel	Table 9	5	10,960	4,750	54	116	249

7.0 CONCLUSION

In this study, a comparative non-linear explicit analysis was performed to study the structural performance of conventional SCS wall subjected to a near-field blast load. Two main parameters of maximum out of plane deformation and PEEQ at the center of the rear plate were considered for comparison. The most effective configuration in terms of concrete strength and plate thickness were identified. The results showed that the rear to the front plate thickness of 1.5 is the optimum ratio to minimize the deformation. In addition, concrete strength more than 100 MPa significantly improved structural performance. Using high strength concrete, instead of normal strength (100 MPA instead of 50 MPa), the rear deformation reduced up to 25%. The effect of concrete density on structural performance was insignificant. Using heavy concrete instead of normal weight and increasing density by 43%, the rear deformation was reduced only by 10%. Two novel configurations were proposed to improve the structural response and were optimized using parametric analysis. The proposed parallel configuration showed significant improvement, when compared to the conventional design. With similar cost fabrication, using the new design, the rear deformation could be reduced up to 44%.

8.0 ACKNOWLEDGMENTS

This financial support for this project was provided by the United States Department of Energy through the Nuclear Energy University Program under the Contract No. 00128931. The findings presented herein are those of the authors and do not necessarily reflect the views of the sponsor.

REFERENCES

[1] Pandey, A., R. Kumar, D. Paul, and D. Trikha, (2006). "Non-linear response of reinforced concrete containment structure under blast loading," *Nuclear Engineering and design*, 236(9): p. 993-1002.

[2] Zhao, C., J. Chen, Y. Wang, and S. Lu, (2012). "Damage mechanism and response of reinforced concrete containment structure under internal blast loading," *Theoretical and Applied Fracture Mechanics*, 61: p. 12-20.

[3] Othman, H., T. Sabrah, and H. Marzouk, (2018). "Conceptual design of ultra-high performance fiber reinforced concrete nuclear waste container," *Nuclear Engineering and Technology*.

[4] Wang, Y., X. Zhai, S.C. Lee, and W. Wang, (2016). "Responses of curved steel-concrete-steel sandwich shells subjected to blast loading," *Thin-Walled Structures*, 108: p. 185-192.

[5] Castedo, R., L. ma Lopez, M. Chiquito, and A.P. Santos, (2019). "Full-scale reinforced concrete slabs: Blast effects, damage characterization and numerical modelling," *International Journal of Safety and Security Engineering*, 9(1): p. 50-60.

[6] Athanasiou, E., F. Teixeira-Dias, F. Coghe, and L. Desmaret, (2016). "Response of reinforced concrete structural elements to near-field and contact explosions," *International Journal of Safety and Security Engineering*, 6(2): p. 418-426.

[7] Kong, S., A. Remennikov, and B. Uy, (2012). "Numerical simulation of high-performance steel-concrete-steel sandwich panels under static and impact loading conditions."

[8] Tabatabaei, Z.S., J.S. Volz, J. Baird, B.P. Gliha, and D.I. Keener, (2013). "Experimental and numerical analyses of long carbon fiber reinforced concrete panels exposed to blast loading," *International Journal of Impact Engineering*, 57: p. 70-80.
[9] Hanifehzadeh, M., B. Gencturk, and K. Willam, *Response of reinforced and sandwich concrete panels subjected to projectile impact*, in *Structures Congress*. 2018: Forth Worth, Texas, USA.
[10] Sawab, J., I. Lim, Y.-L. Mo, M. Li, H. Wang, and M. Guimaraes, *Ultra-High-Performance Concrete And Advanced Manufacturing Methods For Modular Construction.* 2016, Univ. of Houston, Houston, TX (United States).
[11] Sawab, J., C. Luu, X. Nie, I. Lim, Y. Mo, and M. Li, (2016). "Structural integrity of steel plate ultra high-performance concrete modules," *Journal of Structural Integrity and Maintenance*, 1(3): p. 95-106.
[12] Dassault Systemes. *ABAQUS UNIFIED FEA*. (2017) [cited 2017 April 6]; Available from: https://www.3ds.com.
[13] Lee, J. and G.L. Fenves, (1998). "Plastic-damage model for cyclic loading of concrete structures," *Journal of engineering mechanics*, 124(8): p. 892-900.
[14] Dassault Systemes, *ABAQUS*. 2016, Simulia Corp.: Providence, RI, USA.
[15] Bao, X. and B. Li, (2010). "Residual strength of blast damaged reinforced concrete columns," *International journal of impact engineering*, 37(3): p. 295-308.
[16] Hanifehzadeh, M., B. Gencturk, and R. Mousavi, (2018). "A numerical study of spent nuclear fuel dry storage systems under extreme impact loading," *Engineering Structures*, 161(1): p. 68-81.
[17] Mousavi, R., M.D. Champiri, M.S. Joshaghani, and S. Sajjadi, (2016). "A kinematic measurement for ductile and brittle failure of materials using digital image correlation," *AIMS Materials Science*, 3(4): p. 1759-1772.
[18] Mousavi, R., M.D. Champiri, and K.J. Willam, (2016). "A Comparison of Two DamagePlasticity Formulations for Concrete Like Materials."
[19] Hanifehzadeh, M., B. Gencturk, and K. Willam, (2017). "Dynamic structural response of reinforced concrete dry storage casks subjected to impact considering material degradation," *Nuclear Engineering and Design*, 325: p. 192-204.
[20] Jankowiak, T. and T. Lodygowski, (2005). "Identification of parameters of concrete damage plasticity constitutive model," *Foundations of civil and environmental engineering*, 6(1): p. 53-69.
[21] ACI, *Building code requirements for structural concrete and commentary* in *(ACI 318-14) and Commentary (ACI 318-14R)*. 2014, American Concrete Institute (ACI): Farmington Hills, MI.
[22] Bischoff, P.H. and S.H. Perry, (1995). "Impact behavior of plain concrete loaded in uniaxial compression," *Journal of Engineering Mechanics*, 121(6): p. 685-693.
[23] Tang, T., L.E. Malvern, and D.A. Jenkins, (1992). "Rate effects in uniaxial dynamic compression of concrete," *Journal of Engineering Mechanics*, 118(1): p. 108-124.
[24] Weerheijm, J., *Understanding the tensile properties of concrete*. 2013: Elsevier.
[25] Bischoff, P.H. and S.H. Perry, (1991). "Compressive behaviour of concrete at high strain rates," *Materials and Structures*, 24(6): p. 425-450.
[26] CEB-FIP, *Design of Concrete Structures*. 1993, Lausanne, Switzerland: Euro-International Committee for Concrete (CEB).
[27] Cowper, G.R. and P.S. Symonds, *Strain-hardening and strain-rate effects in the impact loading of cantilever beams*. 1957, DTIC Document.
[28] Kingery, C.N. and G. Bulmash, *Airblast parameters from TNT spherical air burst and hemispherical surface burst*. 1984: US Army Armament and Development Center, Ballistic Research Laboratory.
[29] Ruan, Z., L. Chen, and Q. Fang, (2015). "Numerical investigation into dynamic responses of RC columns subjected for fire and blast," *Journal of Loss Prevention in the Process Industries*, 34: p. 10-21.
[30] Talebi, E., M. Korzen, and S. Hothan, (2018). "The performance of concrete filled steel tube columns under post-earthquake fires," *Journal of Constructional Steel Research*, 150: p. 115-128.
[31] Talebi, E., M. Korzen, A. Espinós, and S. Hothan, (2018). "The effect of damage location on the performance of seismically damaged concrete filled steel tube columns at fire."
[32] Shafieifar, M., M. Farzad, and A. Azizinamini, (2017). "Experimental and numerical study on mechanical properties of Ultra High Performance Concrete (UHPC)," *Construction and Building Materials*, 156: p. 402-411.
[33] Sawab, J., L. Mo, and L. Mo. Finite Element Simulation of Steel Plate Ultra High Performance Concrete Composite Modules Subjected to Shear. in *Proceedings of the World Congress on Engineering*. 2016.
[34] Hanif, M., Z. Ibrahim, K. Ghaedi, A. Javanmardi, and S. Rehman, (2018). "Finite Element Simulation of Damage In RC Beams," *Journal of Civil Engineering*, 9(1).
[35] Baghi, H., F. Menkulasi, J. Parker, and J.A. Barros, (2017). "Development of a High-Performance Concrete Deck for Louisiana's Movable Bridges: Numerical Study," *Journal of Bridge Engineering*, 22(7): p. 04017028.